Slip Anticipation for Grasping Deformable Objects Using a Soft Force Sensor

Euan Judd[1], Bekir Aksoy[2], Krishna Manaswi Digumarti[1,2], Herbert Shea[2], Dario Floreano[1]

***Abstract*— Robots using classical control have revolutionised assembly lines where the environment and manipulated objects are restricted and predictable. However, they have proven less effective when the manipulated objects are deformable due to their complex and unpredictable behaviour. The use of tactile sensors and continuous monitoring of tactile feedback is therefore particularly important for pick-and-place tasks using these materials. This is in part due to the need to use multiple points of contact for the manipulation of deformable objects which can result in slippage with inadequate coordination between manipulators. In this paper, continuous monitoring of tactile feedback, using a liquid metal soft force sensor, for grasping deformable objects is presented. The trained data-driven model distinguishes between successful grasps, slippage and failure during a manipulation task for multiple deformable objects. Slippage could be anticipated before failure occurred using data acquired over a 30 ms period with a greater than 95% accuracy using a random forest classifier. The results were achieved using a single sensor that can be mounted on the fingertips of existing grippers and contributes to the development of an automated pick-and-place process for deformable objects.**

I. INTRODUCTION

Robots are yet to replace their human counterparts in environments that contain unpredictable elements. For example, partially predictable environments, such as an assembly line for manufacturing deformable objects, remain a challenge. This is due to the complex and unpredictable behaviour that deformable objects often exhibit. A key aspect of successful manipulation tasks in nature is the continuous monitoring of tactile feedback, including slip anticipation. The importance of this was clearly shown by Johansson et al. [1] who anesthetised human fingertips, significantly impairing their performance on a pick-and-place task. Anticipation of slippage is also important as it can indicate a change in the contact conditions or loading, knowledge of which can be used to adapt the contact normal force. In nature, the normal force during grasping is just above the minimum to prevent slippage, this likely induces small slips that can be used for monitoring these contact conditions [2]. This is needed for tasks that require precision grasping, rather than power grasping, such as manipulating deformable objects. It also avoids sensor saturation which can result in a reduction in sensitivity and dynamic range of the sensors.

There is a rich history of tactile sensors developed to detect slippage. Sensor technologies include optical [3], [4], [5], [6], [7], neuromorphic [8], PolyVinyliDene Fluoride (PVDF) [9], [10], magnetic [11], acoustic [12], accelerometers [13], [14], [15], friction-based [16], capacitive [17], [18], and piezoresistive [19]. The onset of slippage occurs when the shear force is greater than the static friction force. Both the coefficients of static and dynamic friction between two objects in contact are material and system dependant, varying with properties including normal loading and sliding velocity [20]. Slippage is characterised by the frictional force between the two surfaces increasing and decreasing as the objects move relative to each other, this is referred to as the stick-slip phenomenon [21]. However, many of these works focus exclusively on slip detection rather than continuous monitoring of multiple stages of the manipulation task, although some of the sensors would be suitable for both.

The methods for classifying slippage vary from unsophisticated method, such as using a threshold for spikes in sensor readings, to nonlinear data-driven methods. For instance, James et al. [7] compared thresholding, linear and nonlinear support vector classifiers (SVC), and logistic regression using the optical TacTip sensor. Thresholding could be used for classifications [7] but had a significantly lower F1-score (the harmonic mean of the precision and recall) than the more sophisticated data-driven methods. Massalim et al. [13] used deep learning to analyse data from accelerometers embedded in the fingertips of a gripper to classify slippage and texture of a rigid object. Grover et al. [22] mapped barometric tactile sensor data to slippage using a Temporal Convolutional Neural Network (TCN) to extract temporal features from the signals. Kim et al. [15]) transformed the data from a sensor made of piezoelectric material that measures vibration into the frequency domain before using a convolutional neural networks. Veiga et al. [23] used random forests to classify slip with the fluid filled BioTac. An LSTM model was used as the order of the inputs was deemed important. As temporal features are important, most non-LSTM methods provide a window of consecutive samples from the raw data or a spectrogram.

In this paper, we aim to show the continuous monitoring and slip anticipation capabilities of the liquid metal soft force sensor developed in [24]. The soft force sensor can detect the contact normal force as well as shear force for slip anticipation. A data-driven approach was used to classify each stage of a grasping task for deformable objects for continous monitoring, including slip anticipation. We will first introduce the basic working principle of the soft force sensor in section II, then discuss the experimental setup for acquiring a large labelled training dataset in section III, and finally explore the resulting force profiles for grasping

[1]Laberatory of Intelligent Systems, École Polytechnique Fédérale de Lausanne, Switzerland euan.judd@epfl.ch

[2]LMTS: Soft Transducers Lab, École Polytechnique Fédérale de Lausanne, Switzerland

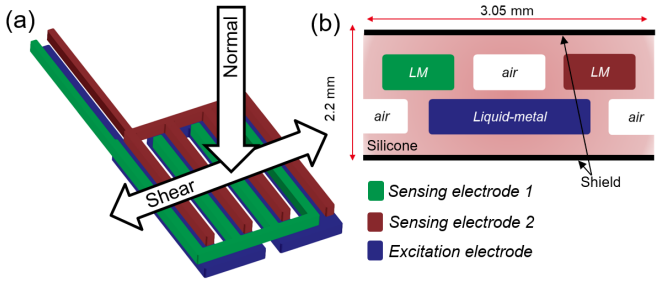

Fig. 1. Liquid metal soft force sensor [24]. (a) The EcoFlex® 00-30 silicone soft force sensor consists of channels partially filled with liquid metal. The capacitances of the two sensing electrodes (green and red) are measured while the excitation electrode (blue) is electrically excited. (b) Cross-section view of the sensor showing a single unit (two sensing electrode channels and one excitation electrode channel) out of the total of four. The relative position of the sensing electrode compared to the excitation electrode changes when a force is applied to the sensor. When a normal force is applied, the distance between the sensing and excitation electrodes decreases. When a shear force is applied, the sensing electrodes shift horizontally.

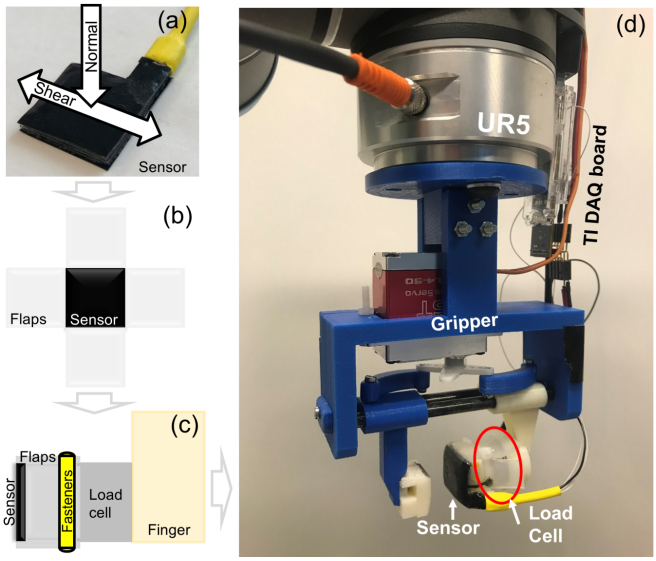

Fig. 2. (a) The soft force sensor was (b) modified to include EcoFlex® 00-30 silicone flaps were adhered to the sensor (SilPoxy, Smooth-On) so that it could be (c) mounted on a finger of the gripper. The flaps also protects the sensor from damage during shear. (d) The modified sensor was mounted on a ATI Nano 17 6-axis load cell on a 1 degree of freedom gripper. The gripper was mounted on a Universal Robotics (UR5) arm. A Texas Instruments FDC1004EVM capacitance data acquisition board was used to read capacitance readings from sensing electrodes 1 and 2 while exciting the excitation electrode.

deformable objects and train various data-driven methods in section IV.

II. HARDWARE

The tactile sensor used in this paper was a liquid metal soft force sensor (Fig. 1) developed by Aksoy et al. [24]. The force sensor is based on capacitive sensing using a unique design. It was fabricated out of EcoFlex® 00-30 silicone with embedded microfluidic channels partially filled with liquid metal (EGaIn). The sensor was electrically shielded on both sides to block any electromagnetic interferences. The grounded shielding was a mixture of carbon particles (CE300, Ketjenblack) and EcoFlex® 00-30. The sensor was designed to sense very small (milli-Newton) normal (F_{normal}) and shear (F_{shear}) forces simultaneously, in the directions shown in Fig. 1(a). It can withstand in excess of 20 N normal force and still give reliable readings.

The relative position of each sensing electrode (1 & 2) compared to the excitation electrode (Fig. 1 green, red & blue, respectively) changes when a force is applied to the sensor. This changes the capacitance between the electrodes, which are read out using a 2-channel capacitance meter. The magnitude of change in capacitance depends on the magnitude and direction of the applied force. The changes in capacitance are then converted to force values using a second order surface fit during calibration. The second order fit for the normal and shear forces, in Newtons, using this sensor are of the form

$$F = a\Delta C_1 + b\Delta C_2 + c\Delta C_1^2 + d\Delta C_1\Delta C_2 + d\Delta C_2^2 \quad (1)$$

where $\Delta C1$ and $\Delta C2$ are the changes in capacitance readings in pF from sensing electrode 1 and sensing electrode 2, respectively. A second order fit was found to sufficiently capture the physics involved. A higher order fit did not result in a significantly lower error. The coefficients a, b, c, d, and e were fit during calibration and were -1.406, -1.227, 0.2465, -1.294, and 0.281 for F_{normal} and -0.824, 0.721, 0.146, -0.076, and -0.148 for F_{shear}, respectively. Notably, these two forces are not decoupled as both are a function of the two capacitance readings, $F_{normal}(\Delta C1, \Delta C2)$ and $F_{shear}(\Delta C1, \Delta C2)$.

Shear force sensitivity is highest when the electrodes can move easily relative to each other. In the original sensor design, the sides of the sensing region were exposed (Fig. 2(a)) which could result in damage to the sensor due to an excessive shear force or the edges of the sensor catching in folds of the manipulated textiles. This was also a potentially significant problem due to the high volume of data that is required for training a data-driven model. A solution was to adhere (SilPoxy, Smooth-On) EcoFlex® 00-30 flaps to the sensing region on four sides (Fig. 2(b) & (c)) and adhere the underside of the sensor to the mechanical gripper using Kapton® Tape. However, while the flaps were necessary for data acquisition, they potentially constrain the relative motion between functional layers which likely reduces the sensitivity of the sensor. An EcoFlex® 00-30 skin was also adhered (SilPoxy, Smooth-On) to the top layer of the sensor that would be in contact with the deformable objects to protect the electrically insulated shielding from wear that could result in more noise in the capacitance readings.

The flaps allowed the sensor to be mounted on an ATI Nano17 6-axis Transducer. The Nano17 was aligned so that the force along the z-axis provided the normal force while

the force along the x-axis provided the shear force. The load cell was used to both compare with the soft force sensor data and to aid in the manual labelling of the training dataset. However, the model that will be trained uses only the soft force sensor data meaning that only the soft force sensor, which has a low profile and can be integrated easily on a mechanical gripper, is needed. The Nano17 was mounted on a bespoke 3D printed gripper (Fig. 2(d)) that used an Arduino Uno controlled KST Coreless X20-8.4-50 servo motor. A Texas Intruments FDC1004EVM 4 Channel Capacitive to Digital Converter Evaluation Module was used to excite the excitation electrode and measure the capacitance of both sensing electrodes. The gripper was mounted on a Universal Robots UR5 arm.

III. DATA ACQUISITION

Continuous monitoring of tactile feedback during grasping of deformable objects is necessary to carry out pick-and-place tasks. In particular, the anticipation of slippage is important so that reactive actions can be taken by other subsystems. A data-driven model will be trained for classifying the tactile sensor data into four categories including (i) gripper open, (ii) successful grasp of object, (iii) object slippage, and (iv) grasp failure causing the object to drop.

The data acquisition process was carefully planned to both produce data that would best approximate the data that would be seen during a pick-and-place task while also allowing for a large number of automated repetitions. Classes (ii) and (iii) need particular attention. Class (ii), successful grasp of an object, will likely be distinguishable from the gripper being closed, but no object grasped, by the increase in the shear force in the former due to the gravitational force on the object's mass. The deformable objects used during acquisition of the training data will therefore need to be free hanging. Slippage, class (iii), will likely occur for many different grasping forces, velocities and angles. For instance, the object will slip at various velocities depending on the velocity of the end effector if the object is under tension. The angle of the slip direction relative to the direction that shear force is most sensitive in the sensor, shown in Fig. 1, will also be an important factor. In addition, slippage will result from an increase in shear force. However, the shear force may increase when the object is under tension but there is no slippage occurring. It is therefore necessary to include data for the object under tension in the successful grasping class (ii), as well as during the slippage class (iii), so that the difference can be learned.

The process, illustrated in Fig. 3, was developed to meet these requirements. First, the open gripper approaches the deformable object hanging below it. The gripper closes and the object is lifted. The object was attached to the same surface as the UR5 arm with sufficient slack in the string that the object is initially free hanging. As the object is lifted, the string reaches it's maximum length at which the object is under tension. The tension is not sufficient to cause slippage and will therefore be treated as an acceptable feature under the successful grasp class (ii). The tension is then reduced by moving the gripper down again before the gripper is once again lifted upwards causing tension to increase until slippage occurs. At this point, the deformable object falls back down to it's starting position and the gripper returns to it's initial position, ready to start the next cycle of the process.

In order for the data-driven model to be generalisable, different contact normal forces, gripper velocities and gripper poses were used for the grasp-slip cycle. A total of 75 combinations were chosen which included 3 grasp forces (1.5, 3 and 4.5 N), 5 velocities (20, 30, 40, 50, and 60 mm/s) and 5 angles (0°, ±10°and ±20°). The grasping normal forces and velocities were chosen to avoid slippage without reducing the sensitivity of the sensor in the former and to match the expected collaborative use case of a person and robot simultaneously manipulating the fabric at a manageable speed for the latter. A total of 500,000 data points were collected by the TI DAQ board at a frequency of 100 Hz. The data is labelled manually by visual inspection of both the force and shear force profiles in Fig. 4(a) & (c), discussed below. This is aided using the change in force between adjacent time steps in Fig. 4(b) & (d).

IV. RESULTS

This section first looks at the profile of the forces from the soft force sensor and then uses this data to train several data-driven models. The former is used for manually labelling the data by visual inspection and the latter aids the selection of the algorithm that is most suitable for this dataset. Inspecting the force profiles also helps illustrate the features of the data that the model may use to distinguish each of the classes.

The normal and shear force readings over a grasp-slip cycle for the soft force sensor are shown in Fig. 4(a) while Fig. 4(c) shows the same forces measured by the load cell. The data from both sensors are comparable in magnitude and both show a negative correlation between the forces. For instance, a rising magnitude in the shear force results in a falling magnitude of the normal force.

As the slip phase progresses in Figs. 4(a) & (c), sharp changes in the magnitude of the forces is visible. This is more easily observed in Figs. 4(b) & (d) which show the change in the forces between successive datapoints. As the slippage progresses (circled in green), the magnitude of the change in force between datapoints increases in the data for both the soft force sensor and the load cell. This is called the stick-slip phenomenon [21] and is characterised by the frictional force between the two surfaces increasing and decreasing repetitively. This change in magnitude is most apparent in the shear force data for both sensors, as would be expected. The sharp changes in magnitude are used for the manual labelling process. The onset of classes (i), (ii), and (iv) are clear from the large spikes in Fig. 4(b) & (d). Slippage is more challenging to label but can also be identified by larger magnitude changes in force between successive samples.

The material of the deformable objects, as well as the parameters for the contact normal force, gripper velocity and pose, all influence the profile of the normal and shear

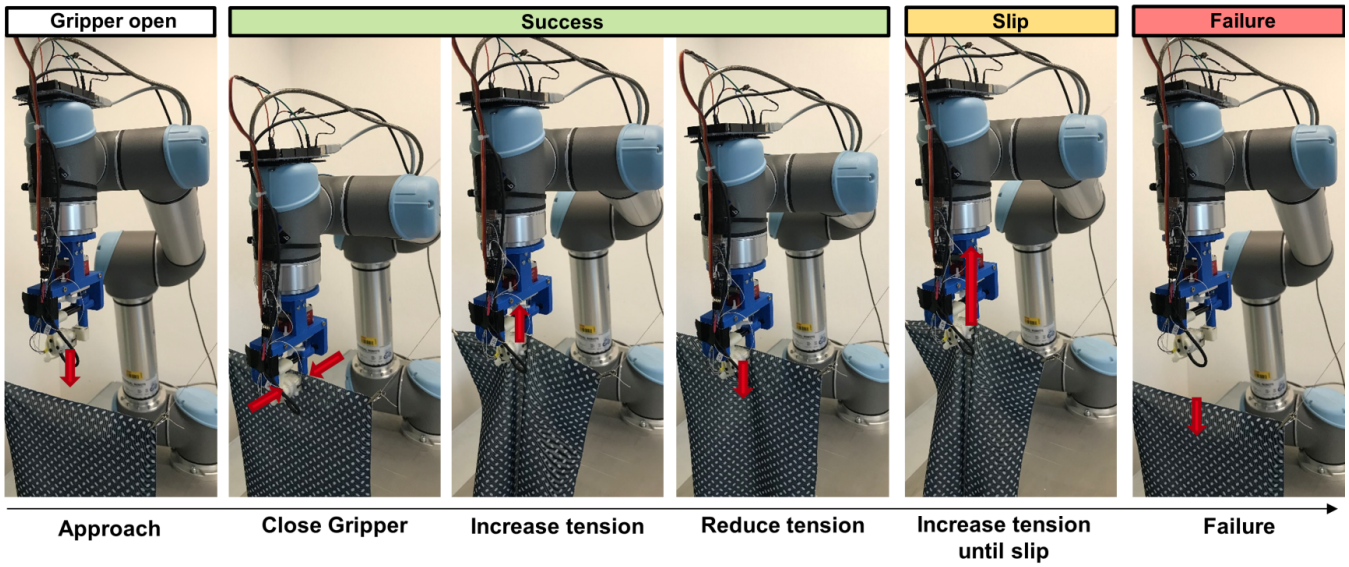

Fig. 3. The repeatable data acquisition process follows six steps. The gripper approaches the object suspended under it. The gripper is closed and the object is lifted upwards and then lowers to cause an increase and then reduction in tension but without slippage. The increase in tension is possible because the object is attached to the same surface as the robot arm. The object is lifted once again until slippage occurs between the two surfaces. After the object has slipped out of the grasp, the gripper remains closed as both the gripper and the object return to the initial positions.

force data (Fig. 5). For instance, the profiles of the forces for the food packaging shows a much sharper rise in the shear force (Fig. 5(b)) compared to the profiles for the fabric (Fig. 5(a)). This is likely due to the fabric stretching as tension is increased while the food packaging, which is flexible but not stretchable, does not.

Each grasp-slip cycle in the dataset were labelled in a similar manner as is seen in Fig. 4. The data was then split into training, validation and testing datasets with a 80%, 10% and 10% split respectively. Each of these datasets was then split into windows of 3 samples where a sample is a pair of forces (F_{normal}, F_{shear}). This corresponds to the algorithm seeing 30 ms of data due to the 100 Hz sampling frequency. This was done so that the algorithms could use the relative change in each of the forces between time steps as well as the relative magnitude of the two forces at any given time step. Window lengths up to 15 samples were tried but did not result in greater accuracy while smaller window sizes had a lower F1-score.

The windows of 3 samples were then inputs to each of the classification algorithms. Logistic regression (LR), support vector classifier (SVC), random forest classifier (RF) [25] were trained using Python's sklearn library and a long short-term memory (LSTM) recurrent neural network (RNN) was trained using Python's keras library. LSTM is the only one of the four that has a temporal component, that is, the order of the samples is important. The other three algorithms take six inputs to the network and use them to estimate the output which, in this case, is the class prediction using one-hot encoding.

LR is a linear method that can be used for classification as it can output a value that corresponds to the probability that an instance belonging to a certain class. It does this by computing a weighted sum of the input features plus a bias term where the weights are learnt during training. A nonlinear SVC was used with a third-degree polynomial kernel function as it performed better than a linear SVC without overfitting the data. The RF is another nonlinear model where the flexibility can be tuned by choosing hyper-parameters such as the maximum depth of each tree, where a greater depth corresponds to a greater flexibility. The LMTS model is a RNN variant where the state of the network is influences both by the most recent datapoint as well as previous datapoints. The recurrent neurons in RNNs feed the output of a previous datapoint back into the network which allows the network to have some memory of past datapoints, although samples that are further back in time have a smaller influence on the current state of the network. This model is therefore both nonlinear and provides a time factor where the order of inputs is important.

Each of these algorithms were trained 5 times and predictions were made using the validation dataset. Fig. 6 shows the mean of the F1-score for each of the algorithms as well as the mean precision, recall and F1-scores in the table. The F1-score is the harmonic mean of the precision and recall

$$F1\text{–}score = 2\frac{(Recall * Precision)}{(Recall + Precision)} \tag{2}$$

where $Precision = TP/(TP + FP)$ and $Recall = TP/(TP + FN)$ where TP is the true positives, FP is the false positives and FN is the false negatives. That is, the precision is the ratio of true positives of a class to all predicted positives while recall is the ratio of true positives of a class to all instances of that class. The F1-score uses the

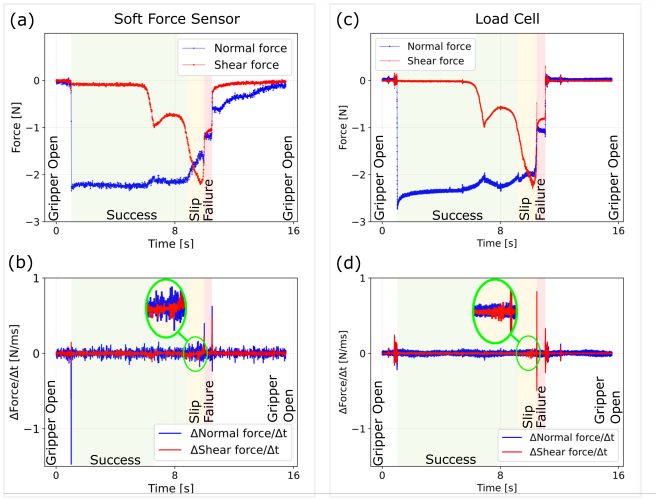

Fig. 4. The forces read from both the soft force sensor and a load cell were used to aid in the manual labelling of the data by visual inspection. (a) F_{normal} and F_{shear} read from the soft force sensor, (b) ΔF_{normal} and ΔF_{shear} between successive time steps for the soft force sensor, (c) F_{normal} and F_{shear} read from the load cell, and (d) ΔF_{normal} and ΔF_{shear} between successive time steps for the load cell. Spikes in (b) and (d) show the onset of the success, failure and the open gripper classes. Slippage was also visible by frequent larger magnitude spikes (circled in green). See each stage of the grasp-slip cycle (colour coded) in Fig. 3.

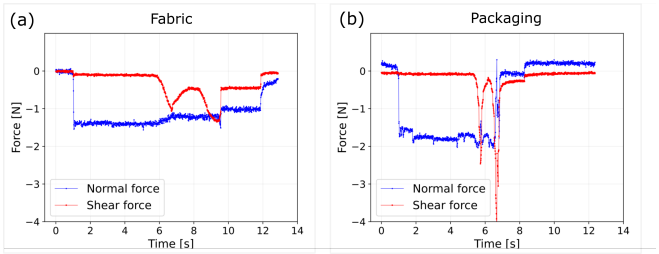

Fig. 5. Each material produces different normal and shear force profiles. (a) shows the force profiles for the fabric while (b) shows the same for the plastic packaging.

harmonic mean as it is sensitive to the lowest values. Finally, the F1-score for a trained model with multiple classes is then the mean of the F1-scores for each of the classes.

LR had an average F1-score of 0.9 showing that a linear model was sufficient to make predictions with this dataset but that the performance could be increased by using a more flexible model (Fig. 6). This suggests that the decision boundary is nonlinear but that the degree of nonlinearity is low. All three nonlinear methods performed similarly well, however the RF classifier had the highest F1-score at 0.955. Therefore, the temporal component of the LSTM did not result in a better performance.

The best RF classifier was then selected as the final model. It was used to make predictions for each of the four classes using the test data (Fig. 7). The F1-score was only 0.6% lower for the test data than for the mean for the validation

	Precision	Recall	F1-score
LR	0.91	0.9	0.9
SVC	0.942	0.939	0.94
LSTM	0.947	0.948	0.948
RF	0.956	0.955	0.955

Fig. 6. Logistic regression, support vector classifier, long short-term memory recurrent Neural Network, and a Random Forest Classifier (RF) were compared using the validation data. A window of 3 data points or 30 ms was sufficient to correctly classify all classes including slippage. The mean precision, recall and F1-scores are shown here. The Random Forest Classifier had the highest mean F1-score although all algorithms had a score greater than 0.9 where 1.0 is the maximum.

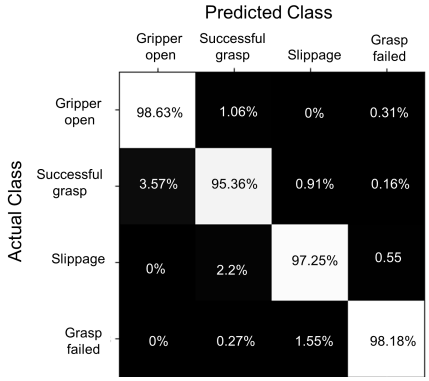

	Test Data Scores
Precision	0.948
Recall	0.95
F1-score	0.949

Fig. 7. The test data confusion matrix for the random forest classifier shows slippage was classified correctly 97.25% of the time. The F1-score on the test dataset was only 0.6% lower than on the validation dataset. The confusion matrix shows an above 95% class prediction accuracy for all classes in the white diagonal.

data. The confusion matrix shows that each of the classes were classified correctly at least 95.36% of the time. Slippage was classified correctly 97.25% of the time.

Confusion most often occurred with the successful grasp class (ii) which was most often incorrectly predicted as the gripper open class (i). This likely occurs at lower contact normal forces when the difference between the gripper being open and gripper closed on the object is lowest. The 30 ms window of data was sufficient to anticipate slippage which had a total duration greater than 1000 ms depending on the velocity of the gripper. This gives sufficient time to detect slippage, verify the class by waiting until several successive predictions corroborate the first, and then performing a reactive action to stop slippage from continuing.

V. CONCLUSION

The work in this paper shows the continuous monitoring capabilities of a previously developed novel soft force sensor for continuous monitoring of tactile feedback, including slip anticipation. The results highlight the usefulness of continuously monitoring tactile feedback from this soft force sensor during the manipulation of deformable objects, such as textiles, during pick-and-place tasks. This is a particularly

challenging problem due to the complex and unpredictable behaviour of deformable objects. It was shown that each stage of the grasping procedure was successfully predicted using the trained data-driven model with a greater than 95% accuracy. Slippage was successfully predicted with 97.25% accuracy using just 30 ms of data, allowing rapid anticipation of slippage. The trained model is also generalisable in that it can successfully make predictions when the contact normal forces, gripper poses and slip velocities are varied. Various data-driven methods were compared to find the appropriate method for successfully classifying each stage of the grasping task. Nonlinear methods performed better than less flexible models with the random forest classifier having the highest F1-score. The sensor used in this paper was sufficiently sensitive to detect small fluctuations in the force profiles due to slippage when the contact normal force was low. Each stage of the manipulation task was monitored using a single soft force sensor that can be mounted on an existing gripper. Our method of continuous force monitoring and slip anticipation is a key step towards the use of robots in assembly lines where they are tasked with grasping and manipulation soft, fragile and deformable materials.

ACKNOWLEDGMENT

This project has received funding from the European Union's Horizon 2020 research and innovation programme under grant agreement No 869963 (MERGING).

REFERENCES

[1] R. S. Johansson and J. R. Flanagan, "Coding and use of tactile signals from the fingertips in object manipulation tasks," *Nature Reviews Neuroscience*, vol. 10, no. 5, pp. 345–359, 2009.

[2] R. S. Johansson and G. Westling, "Roles of glabrous skin receptors and sensorimotor memory in automatic control of precision grip when lifting rougher or more slippery objects," *Experimental brain research*, vol. 56, no. 3, pp. 550–564, 1984.

[3] K. Kamiyama, H. Kajimoto, M. Inami, N. Kawakami, and S. Tachi, "A vision-based tactile sensor," in *International Conference on Artificial Reality and Telexistence*, pp. 127–134, 2001.

[4] H. Khamis, B. Xia, and S. J. Redmond, "A novel optical 3d force and displacement sensor–towards instrumenting the papillarray tactile sensor," *Sensors and Actuators A: Physical*, vol. 291, pp. 174–187, 2019.

[5] J. W. James, N. Pestell, and N. F. Lepora, "Slip detection with a biomimetic tactile sensor," *IEEE Robotics and Automation Letters*, vol. 3, no. 4, pp. 3340–3346, 2018.

[6] S. Dong, W. Yuan, and E. H. Adelson, "Improved gelsight tactile sensor for measuring geometry and slip," in *2017 IEEE/RSJ International Conference on Intelligent Robots and Systems (IROS)*, pp. 137–144, IEEE, 2017.

[7] J. W. James and N. F. Lepora, "Slip detection for grasp stabilization with a multifingered tactile robot hand," *IEEE Transactions on Robotics*, vol. 37, no. 2, pp. 506–519, 2020.

[8] A. Rigi, F. Baghaei Naeini, D. Makris, and Y. Zweiri, "A novel event-based incipient slip detection using dynamic active-pixel vision sensor (davis)," *Sensors*, vol. 18, no. 2, p. 333, 2018.

[9] D. Goeger, N. Ecker, and H. Woern, "Tactile sensor and algorithm to detect slip in robot grasping processes," in *2008 IEEE International Conference on Robotics and Biomimetics*, pp. 1480–1485, IEEE, 2009.

[10] C. Choi, W. Schwarting, J. DelPreto, and D. Rus, "Learning object grasping for soft robot hands," *IEEE Robotics and Automation Letters*, vol. 3, no. 3, pp. 2370–2377, 2018.

[11] S. Takenawa, "A magnetic type tactile sensor using a two-dimensional array of inductors," in *2009 IEEE International Conference on Robotics and Automation*, pp. 3295–3300, IEEE, 2009.

[12] H. Shinoda, K. Matsumoto, and S. Ando, "Acoustic resonant tensor cell for tactile sensing," in *Proceedings of International conference on Robotics and Automation*, vol. 4, pp. 3087–3092, IEEE, 1997.

[13] Y. Massalim, Z. Kappassov, and H. A. Varol, "Deep vibro-tactile perception for simultaneous texture identification, slip detection, and speed estimation," *Sensors*, vol. 20, no. 15, p. 4121, 2020.

[14] R. D. Howe and M. R. Cutkosky, "Sensing skin acceleration for slip and texture perception.," in *ICRA*, pp. 145–150, 1989.

[15] S. J. Kim, S. H. Lee, H. Moon, H. R. Choi, and J. C. Koo, "A non-array type cut to shape soft slip detection sensor applicable to arbitrary surface," *Sensors*, vol. 20, no. 21, p. 6185, 2020.

[16] P. Dzitac, A. M. Mazid, M. Y. Ibrahim, G. K. Appuhamillage, and T. A. Choudhury, "Friction-based slip detection in robotic grasping," in *IECON 2015-41st Annual Conference of the IEEE Industrial Electronics Society*, pp. 004871–004874, IEEE, 2015.

[17] H. Yang, X. Hu, L. Cao, and F. Sun, "A new slip-detection method based on pairwise high frequency components of capacitive sensor signals," in *2015 5th International Conference on Information Science and Technology (ICIST)*, pp. 56–61, IEEE, 2015.

[18] A. Narendiran and B. George, "Capacitive tactile sensor with slip detection capabilities for robotic applications," in *2015 IEEE International Instrumentation and Measurement Technology Conference (I2MTC) Proceedings*, pp. 464–469, IEEE, 2015.

[19] M. Meier, F. Patzelt, R. Haschke, and H. J. Ritter, "Tactile convolutional networks for online slip and rotation detection," in *International Conference on Artificial Neural Networks*, pp. 12–19, Springer, 2016.

[20] W. Chen, H. Khamis, I. Birznieks, N. F. Lepora, and S. J. Redmond, "Tactile sensors for friction estimation and incipient slip detection—toward dexterous robotic manipulation: A review," *IEEE Sensors Journal*, vol. 18, no. 22, pp. 9049–9064, 2018.

[21] E. Rabinowicz, "The intrinsic variables affecting the stick-slip process," *Proceedings of the Physical Society (1958-1967)*, vol. 71, no. 4, p. 668, 1958.

[22] A. Grover, C. Grebe, P. Nadeau, and J. Kelly, "Under pressure: Learning to detect slip with barometric tactile sensors," *arXiv preprint arXiv:2103.13460*, 2021.

[23] F. Veiga, J. Peters, and T. Hermans, "Grip stabilization of novel objects using slip prediction," *IEEE transactions on haptics*, vol. 11, no. 4, pp. 531–542, 2018.

[24] B. Aksoy, Y. Hao, G. Grasso, K. M. Digumarti, V. Cacucciolo, and H. Shea, "Shielded soft force sensors - under review," 2022.

[25] L. Breiman, "Random forests," *Machine learning*, vol. 45, no. 1, pp. 5–32, 2001.